Non-asymptotic transients away from steady states determine cellular responsiveness to dynamic spatial-temporal signals

Akhilesh Nandan[1] and Aneta Koseska[1,*]

[1]*Cellular computations and learning, Max Planck Institute for Neurobiology of Behavior – caesar, Ludwig-Erhard-Allee 2, 53175 Bonn, Germany*

Abstract

Majority of the theory on cell polarization and the understanding of cellular sensing and responsiveness to localized chemical cues has been based on the idea that non-polarized and polarized cell states can be represented by stable asymptotic switching between them. The existing model classes that describe the dynamics of signaling networks underlying polarization are formulated within the framework of autonomous systems. However these models do not simultaneously capture both, robust maintenance of polarized state longer than the signal duration, and retained responsiveness to novel signals. Using recent experimental evidence for criticality organization of biochemical networks, we challenge the current concepts and demonstrate that non-asymptotic signaling dynamics arising at criticality uniquely ensures optimal responsiveness to changing chemoattractant fields. We provide a framework to characterize non-asymptotic dynamics of system's state trajectories through a non-autonomous treatment of the system, further emphasizing the importance of (long) transient dynamics, as well as the necessity to change the mathematical formalism when describing biological systems that operate in changing environments.

Keywords cell polarization | responsiveness to changing signals | dynamical "ghost" states | non-autonomous systems | non-asymptotic transient dynamics | criticality

Introduction

During embryogenesis, wound healing, or cancer metastasis, cells continuously sense and chemotactically respond to dynamic spatial-temporal signals from their environment (Barton et al., 2016; Shellard and Mayor, 2016; Lämmermann et al., 2013; Samara et al., 2011). This response is based on cell polarization - the formation of a distinct front and back of the cell through stabilization of polarized signaling activity at the plasma membrane. Broad range of cells, including epithelial or nerve cells, fibroblasts, neutrophils, *Dictyostelium discodeum* etc., display multiple common polarization features: quick and robust polarization in the direction of the localized signal, sensing of steep and shallow gradients (and subsequent amplification of the internal signaling state between the opposite ends of the cell), as well as threshold activation as a means to filter out noise (Welf et al., 2012; Jilkine and Edelstein-Keshet, 2011). Moreover, polarity and thereby directional migration is transiently maintained after the trigger stimulus is removed (memory in polarization), but the cells remain sensitive to new stimuli, and can rapidly reorient when the signal's localization is changed. In response to multiple stimuli such as two sources with varying concentrations, rapid resolution with a unique axis of polarity towards the signal with higher concentration is ensured (Welf et al., 2012).

A large diversity of models, both abstract and biochemically detailed have been proposed, however none of them can account for all of the common experimentally observed features. For example, the local excitation global inhibition model (LEGI) (Levchenko and Iglesias, 2002; Parent and Devreotes, 1999) and its variants (Levine et al., 2006; Xiong et al., 2010; Skoge et al., 2014) rely on an incoherent feed-forward motif, whose dynamics doesn't account for transient memory in polarization. The Turing-like models based on a local activation long-range inhibition (activator-inhibitor system) (Otsuji et al., 2007; Goryachev and Pokhilko, 2008) are not robust to noise, cannot resolve simultaneous signals in physiologically relevant time frame (Jilkine and Edelstein-Keshet, 2011) or maintain responsiveness to upcoming signals. The Wave-pinning model based on a higher-order nonlinear positive feedback, also cannot capture responsiveness to subsequent signals (Mori et al., 2008; Edelstein-Keshet et al., 2013; Mori et al., 2010). Thus, to capture the experimentally observed polarization features in a single model, we have recently proposed a mechanism (referred to as a SubPB mechanism) that relies on critical organization to a saddle-node which stabilizes a subcritical pitchfork

*To whom the correspondence should be addressed. Email: aneta.koseska@mpinb.mpg.de

(PB) bifurcation (SN_{PB}) (Nandan et al., 2022). We have demonstrated also experimentally using the Epidermal growth factor receptor (EGFR) network that such organization is crucial for navigation in changing environments.

We take here the conceptual basis of polarity one step further: we argue that cell polarization and responsiveness necessary for navigation in changing spatial-temporal chemoattractant fields is a highly dynamic transient process, and must be studied via an explicit time-dependent form, or as a non-autonomous process. For non-autonomous systems, both the number and the position of steady state change, implying that the steady-state behavior alone does not fully capture the dynamics of the system. What is most relevant are therefore the trajectories representing the change of the state of the system that follow the steady-state landscape changes. This conceptual shift enables to consider transients explicitly, and we demonstrate that a pure non-autonomous succession of steady states, as characteristic for the LEGI, Turing-like or Wave-pinning models cannot explain both transient memory in cell polarization and cellular responsiveness to upcoming signals. On the other hand, non-asymptotic transient states that arise due to organization at criticality as in the SubPB mechanism enable to maintain the dynamics of the sensing network away from a fixed point, and uniquely confer optimal sensing and responsiveness to cells that operate in a changing environment. We therefore argue that the formal descriptions how cells sense and respond to dynamic signals must be modified to consider also (long) non-asymptotic tranisent processes.

Results

Studying cell polarity response as transients in non-autonomous systems

To investigate the dynamical characteristics of polarization, we consider a generalized one dimensional reaction diffusion (RD) system with two components u and v,

$$\begin{aligned} \frac{\partial u(\theta,t)}{\partial t} &= f_u(u,v) + D_u \frac{\partial^2 u}{\partial \theta^2} + s(\theta,t)v \\ \frac{\partial v(\theta,t)}{\partial t} &= f_v(u,v) + D_v \frac{\partial^2 v}{\partial \theta^2} \end{aligned} \tag{1}$$

where $\theta, t \in R$ are angular position on the plasma membrane of a cell with respect to its center and time, $f_u, f_v : R \times R \to R$ are the reaction terms of u and v respectively, D_u and D_v - the diffusion constants, and $s(\theta,t)$ - the distribution of the external chemoattractant signal with respect to the cell. The reaction term $f_u(u,v)$ is chosen as for the Wave-pinning model (Mori et al., 2008), exemplifying a Rho-GTPase cycle with an inter conversion between its active, membrane bound (u) and inactive, cytosolic (v) components (Fig. 1A, top):

$$f_u(u,v) = (k_0 + \gamma u^2/(K^2 + u^2))v - \delta u \tag{2}$$

and $f_v = -f_u$ due to mass conservation ($u + v = c_{total}$). The positive feedback from u onto its own production (via GEFs) is represented by a Hill function of order 2 with maximal conversion rate γ and saturation parameter K, k_0 is a basal GEF conversion rate and δ is the constant inactivation rate (via GAPs). The analytical conditions for the existence of a sub-critical pitchfork bifurcation and a corresponding critical organization can be described in two parts (Nandan et al., 2022), the conditions for the existence of a pitchfork (PB), and the existence of a saddle-node bifurcation (SN_{PB}) through a combination of linear stability analysis, and a weakly non-linear analysis (Materials and Methods). For simplicity of the analysis, we consider a one dimensional projection of the system, assuming two compartments (left and right) having a diffusive exchange (Fig. 1A bottom, Eq. (7)).

The analytical as well as the numerical bifurcation analysis (Ermentrout, 2002) demonstrated that, in absence of a signal ($s(\theta,t) = 0$), the system exhibits a sub-critical PB that is stabilized via $SN_{PB}s$ at a critical total concentration of the system's constituents ($c_{total}^{critical}$, Fig. 1B). The PB generates a transition from a non-polar or homogeneous steady state (HSS, $u_{left,s} = u_{right,s}$, $v_{left,s} = v_{right,s}$), to a polar state represented as a inhomogeneous steady state (IHSS). The IHSS is manifested via two symmetric branches - a combination of a high receptor phosphorylation at the cell left and low at the right side of the cell ($u_{right} < u_{left}$ or left-polarized (top branch)), and $u_{right} > u_{left}$ or right-polarized (lower branch). This demonstrates that the SubPB mechanism can explain robust non-polar and polar states. When the system is organized at criticality (before SN_{PB}, shaded region in Fig.1B), a transient gradient stimulus implemented in the RD simulation reveals rapid u-activity polarization in the direction of the maximal chemoattractant concentration, which is transiently maintained after signal removal (spatial signal and response kymograph in Fig. 1C).

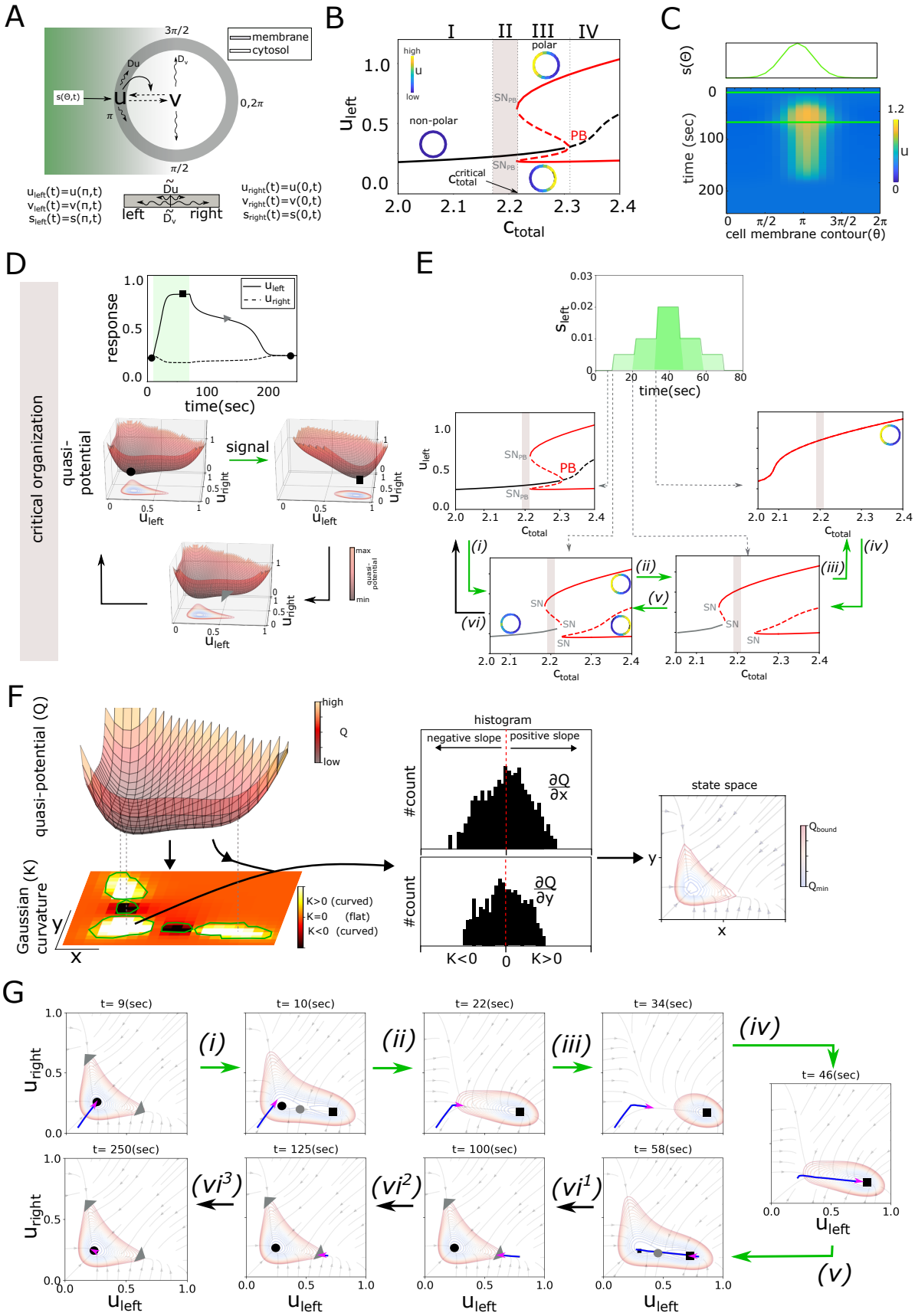
A
3π/2
membrane
cytosol
Du
Dv
s(Θ,t)
u
v
0,2π
π
π/2
uleft(t)=u(π,t)
vleft(t)=v(π,t)
sleft(t)=s(π,t)
Du
left
Dv
right
uright(t)=u(0,t)
vright(t)=v(0,t)
sright(t)=s(0,t)
B
I
II
III
IV
high
u
low
polar
non-polar
SNPB
PB
uleft
ctotal
critical ctotal
C
s(Θ)
time (sec)
cell membrane contour(θ)
u
D
critical organization
response
time(sec)
uleft
uright
quasi-potential
signal
max
min
E
sleft
time(sec)
SNPB
PB
SN
(i)
(ii)
(iii)
(iv)
(v)
(vi)
F
quasi-potential (Q)
high
Q
low
Gaussian curvature (K)
K>0 (curved)
K=0 (flat)
K<0 (curved)
histogram
negative slope
positive slope
#count
∂Q/∂x
∂Q/∂y
K<0
0
K>0
state space
Qbound
Qmin
G
t= 9(sec)
t= 10(sec)
t= 22(sec)
t= 34(sec)
t= 46(sec)
t= 58(sec)
t= 100(sec)
t= 125(sec)
t= 250(sec)
(vi1)
(vi2)
(vi3)

Figure 1: Describing polarization response using transients in a non-autonomous system. (A) Top: Schematic representation of the two component ($u(\theta,t)$ - membrane bound, $v(\theta,t)$ - cytosolic) reaction-diffusion system (Eq. (1)) of a circular cell stimulated with spatial chemical gradient $s(\theta,t)$. (0-2π): angular positions with respect to cell center. Solid/dashed arrows: causal/conversion link. Curly arrows: diffusion. Bottom: respective one dimensional projection of the model (Eq. (7)). (B) Bifurcation diagram of the system in (A) bottom, with respect to the total protein concentration c_{total} for $s(\theta,t)=0$. Dotted lines: regions I-IV with qualitatively different dynamical response; solid /dashed lines: stable/unstable homogeneous (black) and inhomogeneous (red) steady states. Insets: schematic representations of the homogeneous/inhomogeneous signaling states. PB: Pitchfork bifurcation, SN_{PB}: Saddle-node of a pitchfork bifurcation. Shaded region: criticality. (C) Spatial chemoattractant distributions (top) and the corresponding kymograph of $u(\theta,t)$, obtained using RD simulation of the system in (A) top, for organization at criticality (region II in (B)). Green horizontal lines: gradient duration. (D) Top: Time series of the u-signaling response (corresponding to (C)). Green shaded region: interval of gradient signal. Circle/square/triangle: non-polar/polar/transient-polar (memory) state. Bottom: Respective quasi-potential landscape transitions. Coloured contour maps: landscape projections in u_{left}-u_{right} plane. See also Supplementary Fig.2. Green/black arrows:transitions during signal presence/absence. (E) Unfolding of the PB in the presence of a spatial step-like signal ($s_{left}=0.02$ maximal amplitude, $s_{right}=0.0$). The bifurcation diagram for each step-wise increment is shown. Green/black arrows as in (D). Line descriptions as in (B). (F) Representation of Gaussian curvature estimate of a quasi-potential landscape (left), schematic representation of the subsequent slope distributions for distinct landscape regions (middle) and resulting contours determining the phase space region characterised with asymptotic behavior of the system's trajectory (right). See also Supplementary Fig. 1C. (G) Corresponding instantaneous phase portraits with the integrated progression of the trajectory (blue line) during the last 40s before signal change. Pink arrow: current trajectory position and direction. Black/grey circles: HSS/saddle; squares - IHSS; triangles - dynamical "ghost" / memory state.

To verify that the transient memory in polarization emerges from a 'ghost' of the SN_{PB} as described in (Nandan et al., 2022), we used the one-dimensional model to calculate the quasi-potential landscapes that depict the energy-like levels associated with the states (Fig. 1D; Materials and Methods; and (Verd et al., 2013; Wang et al., 2010)). For the critical organization, in absence of a signal, only the HSS (the non-polar state) is stable, manifested through the presence of a single well (Fig. 1D, HSS: circle). However, since the system is positioned close to the critical transition towards the IHSS, the landscape has a shallow area in this region. Upon signal addition, the HSS is lost and the IHSS (square) is stabilized, causing the transition to the newly established well. The opposite transition then takes place upon signal removal, but in this case, the system is initially transiently trapped in the formed shallow region of the landscape (triangle), resulting in a slow time-scale which is manifested as a transient memory of the polarized state.

The observed change of the topology of the system's phase space suggests that cell polarization should be formally treated as a non-autonomous process. In general, in non-autonomous systems, either the geometry (change in the positioning, shape and size of the attractors), or the topology (change in the number or stability of the attractors) of the underlying phase space is altered (Verd et al., 2013). Thus, to understand the associated changes in the number and stability of the attractors in the presence of transient signals, we took a step-like approximation approach to the change in the parameter values by assuming a spatial input (i.e. s_{left}, Fig. 1E) that is discreetly increased/decreased. Calculating the bifurcation diagram for each of the discrete time steps reveals how its structure is modified: even a low-amplitude spatial signal (step *(i)*) introduces an asymmetry to the system and thereby a universal unfolding of the PB (Golubitsky and Schaeffer, 1985), such that a marginally asymmetric steady state (Fig. 1E, gray solid lines) replaces the HSS (black solid lines in signal absence). Moreover, for the same parameter values, now also the IHSS (a remnant of the PB that disappeared) is also stable. Increasing the spatial signal's amplitude in the next steps leads to an increase in the extent of the unfolding, rendering the IHSS as the only stable solution at the maximal signal strength (step *(iii)* in Fig. 1E). This solution corresponds to the single-well landscape in Fig. 1D, representing a robust polarization of the system. Decreasing the signal amplitude in the same step-wise manner results in the reversed changes in the bifurcation diagram structure, thereby explaining the resetting the system to the non-polar HSS after signal removal.

It is important to note here that although the respective branches are stabilized via SN bifurcations upon the unfolding of the PB, this is not equivalent to a generic bistable system, where the SNs lead to emergence of two HSSs. The fundamental difference lies in the nature of the steady states itself. HSS align along the non-polar diagonal axis in the (u_{left}-u_{right}) phase space, while the IHSS along the polar axis perpendicular to it (Supplementary Fig. 1A), which is accessible through unfolding of the PB. To demonstrate that the nature of the steady states emerging via SNs due to the non-autonomous nature of the system and the subsequent unfolding of the PB in a two-dimensional system are not equivalent to generic bistable system, we performed equivalent analysis on a bistable model system which, in absence of a signal, does not exhibit a PB (Eq. (21), Supplementary Fig. 1B, left). In this case, two HSSs are stabilized via SN bifurcations, where a transient signal introduces a switch from the lower to the upper HSS (Supplementary Fig. 1B,

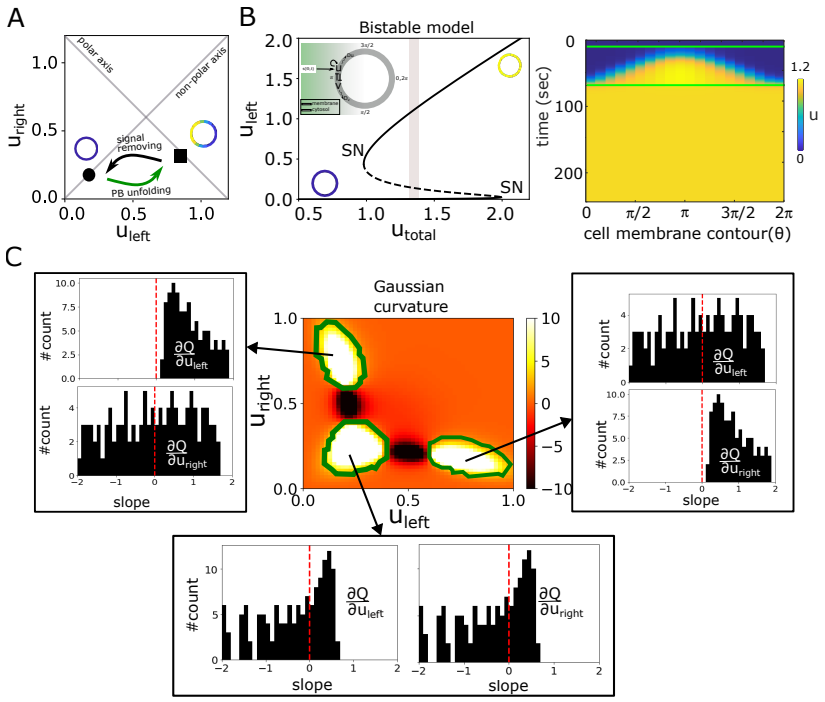

Supplementary Figure 1: Characterizing non-autonomous state transitions for the model in Fig.1A and a bistable polarity model. (A) Phase-plane positioning of the IHSS attractor (square) and the marginally asymmetric steady state (circle) during PB unfolding. (B) Left: Bifurcation diagram of a RD model (inset, Eq. (21)) displaying bistability in signal absence. Lines and coloring as in Fig.1A, B. Grey shaded region: parameter organization. Right: corresponding u-response upon transient gradient stimulation (gradient duration: green horizontal lines). Kymograph obtained from RD simulation of Eq. (21). (C) Exemplary estimate of Gaussian curvature (middle) and corresponding slopes distribution in $(x, y) = (u_{left}, u_{right})$ direction for each of the identified regions. Slopes distribution around 0 in both direction in conjunction with positive curvature uniquely determines a well (stable steady state) in the potential landscape. Description as in Fig.1F.

right). Polarized signaling along the membrane is only observed initially, due to the spatial localization of the signal. However, as a result of the diffusion of the network components along the membrane, the polarization is not spatially confined, leading to a uniformly active state that is further maintained after signal removal as a consequence of the organization in the bistable regime.

The non-autonomous treatment of the systems thus allowed us to track the changes in the number and stability of the attractors, however the fixed point analysis does not capture the full dynamics of the system, as the memory emerging from the SN_{PB} 'ghost' cannot be examined in this analysis. This implies that the transient dynamics of the system must be considered explicitly, through the trajectories of the system which represent the change of the state of the system. To classify the nature of the transients, it is necessary to quantify the phase space regions in which the steady states asymptotically bind the trajectories. For this, we calculated the Gaussian curvature of the quasi-potential landscapes for each step of the signal (schematic in Fig. 1F, left). A surface has a positive curvature ($K > 0$) at a point if the surface curves away from that point in the same direction relative to the tangent to the surface, a negative ($K < 0$) - if the surface curves away from the tangent plane in two different directions, and a $K \sim 0$ - a flat surface. Complementing the curvature calculations with the slopes along each point (e.g. for a well, positive curvature and slope values distributed around 0 are a unique identifier, Fig. 1F, middle; Supplementary Fig. 1C) allowed to identify the phase space region where the trajectory asymptotically moves towards the steady state (contour plot in Fig. 1F, right). Thus, movement of the system's trajectory in areas outside of these regions correspond to a non-asymptotic, transient dynamics of the system. Detailed phase plane analysis of the system for each interval in the step-like spatial signal showed that during transition *(i)*, the marginally asymmetric steady state and the IHSS are stable (as shown in as in Fig.1E), whereas the system's trajectory is trapped in the former one (Fig. 1G). In the next steps *(ii, iii)*, only the IHSS attractor is stable but moves its position. The trajectory's current state falls behind and reacts by travelling towards the moving attractor. Since the flow rate along the trajectory is smaller than the velocity of the attractor movement, the system is not able to catch up with the moving steady state and temporally reverts from asymptotic to transient behaviour. The trajectory is

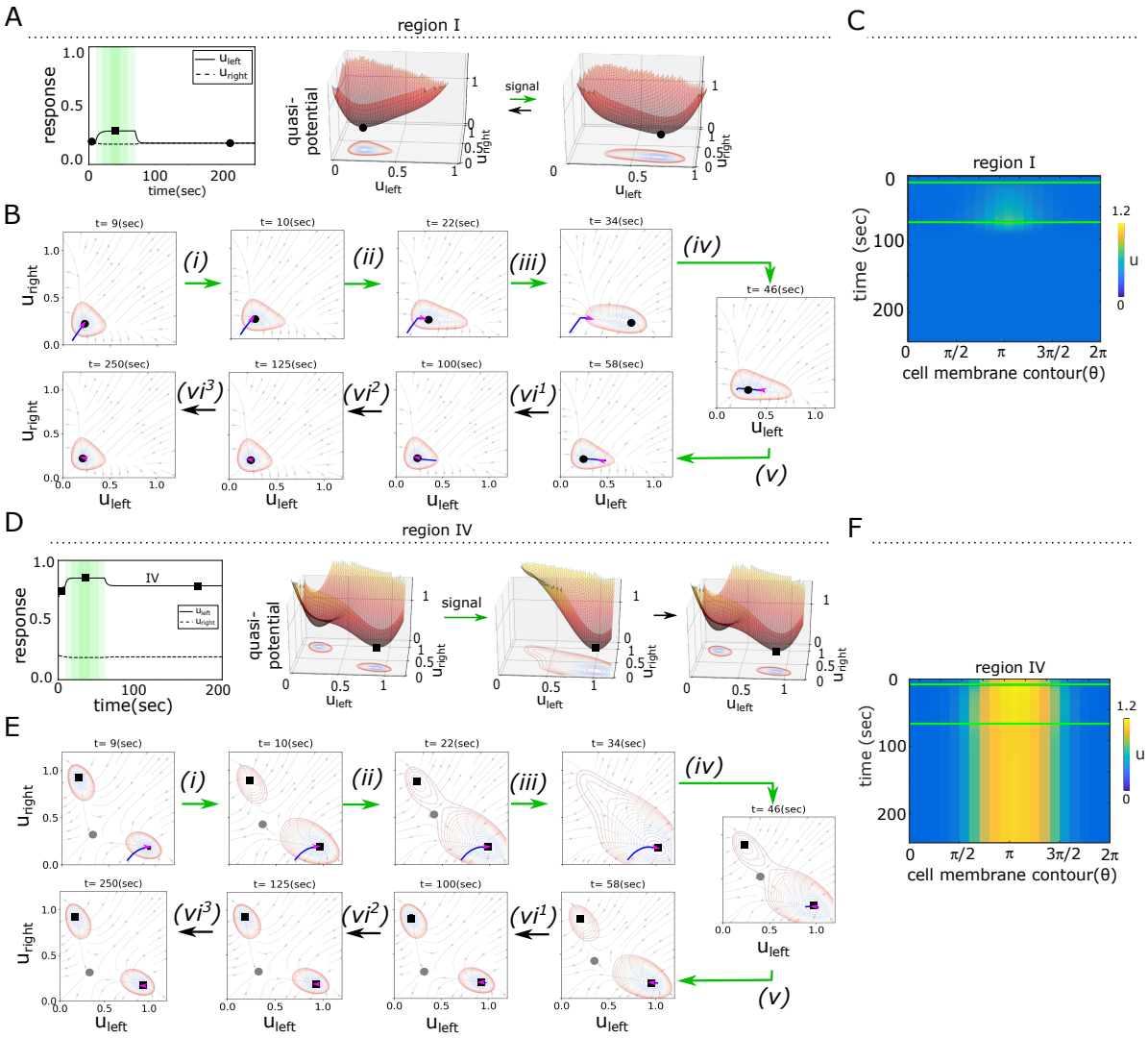

Supplementary Figure 2: Characterizing non-autonomous state transitions for regions I and IV, corresponding to Fig.1B. (A) Left: Time series of the u-signaling response of the SubPB model upon step-like gradient signal (green-shaded region), for organization in region I. Right: Corresponding quasi-potential landscape for $s = 0$ and at the maximal amplitude ($s_{left} = 0.02$). (B) Corresponding instantaneous phase portraits and system's trajectory. Symbols/coloring as in Fig.1G. (C) Corresponding spatial-temporal u-activity response. (D)-(F) Same as in (A)-(C), only for organization in region IV.

asymptotically bounded to the IHSS only at the highest signal strength (step *(iv)*). Decreasing the signal strength leads to re-appearance of the marginally asymmetric state, whereas the IHSS moves from the previous step, such that the trajectory reverts the direction to follow the attractor (step *(v)*). At a zero signal amplitude, the topology of the landscape changes again such that a single stable HSS is generated. In the position where the IHSS attractor was lost however, the landscape is characterized with a shallow slope ("ghost" of the SN_{PB}, triangle in Fig. 1G). This lies right outside the border determining the asymptotic behavior, and the system's trajectory not only lags behind, but it is effectively trapped in this state for a transient period of time (*(vi*^{1}*, vi*^{2}*)*) resulting in transient memory of the polarized state, before it quickly reverts to the HSS attractor (*(vi*^{3}*)*). Thus, examining transient dynamics during the signal-induced transition reveals important details that shape the trajectory, and hence the response of the system, that could not be understood by focusing only on the steady state behaviour.

We have performed equivalent explicit time-dependent analysis also for organization of the system in the remaining regions in the bifurcation diagram (I and IV in Fig. 1B) that we briefly describe here for completeness. For organization in region I, the only stable solution in absence of a signal is a homogeneous distribution of u across the cell membrane.

Step-wise signal amplitude increase only shifts the position of this steady state (change in the geometry of the landscape), and the system displays asymptotic behavior (Supplementary Fig. 2A-C). Similar behavior is also observed for organization in region IV, only in this case the system is in the IHSS even in the absence of the signal (pre-polarized state), and remains in this state during and after signal removal (Supplementary Fig. 2D-F). This demonstrates that for organization in region I and IV, the behavior of the system is not governed by transient dynamics. Organization in region III on the other hand corresponds to the Wave-pinning mechanism, and we therefore discuss this in conjunction with the LEGI and the Turing-like models in the next section.

Non-autonomous succession of steady states underlies the dynamics of the existing polarity models

The bifurcation analysis for the three characteristic model-classes was performed using linear perturbation analysis (LPA), method that allows to identify the dynamical transitions in RD models characterized with large disparity between the diffusivity of the system's components (Holmes et al., 2015; Veronica, 2009). In brief, the LPA enables to approximate the PDE with an ODE model that describes the evolution of a local perturbation (u_{local}) of the slow diffusing component, allowing thereby to probe the stability of a HSS of such system (see Materials and Methods for details). As can be already deduced by the LEGI network topology, the incoherent feed-forward motif, this model has a single HSS (Fig. 2A, shaded region: respective parameter organization as used in the literature (Levchenko and Iglesias, 2002; Levine et al., 2006)). The Turing-like model on the other hand displays a transcritical bifurcation (TC) at a critical total concentration of the system's constituents. The TC marks a transition from non-polar HSS to a polarized, symmetry-broken state. In the literature (Otsuji et al., 2007; Goryachev and Pokhilko, 2008), the model is parameterized after the TC, where the HSS is unstable (Fig. 2B, shaded region: parameter organization). The Wave-pinning model, as already described in (Mori et al., 2008), is characterized by a sub-critical PB, but in contrast to the SubPB model, it is organized in the region where the HSS and the IHSS co-exist (Fig. 2C, shaded region; equivalent to region III in Fig. 1B). RD simulations of these models, consistent with previous findings, revealed that upon transient gradient stimulation, the LEGI model shows a transient polarization that decays to homogeneous non-polar activity distribution immediately after stimulus removal. In contrast, both Turing-like and Wave-pinning models showed a long-term maintenance of the polarized response after signal removal (Supplementary Fig. 3A).

Considering the time-dependence explicitly in the analysis shows that the trajectory describing the state of the LEGI model exposed to transient, step-like spatial signal asymptotically follows the change in the position of the only steady state of the system, thereby marking the steady-state as the only relevant behavior (Fig. 2D,E; Supplementary Fig. 3B left). As noted by the bifurcation analysis, the Turing-like model is organized in the stable symmetry-broken state, thereby cannot describe a stable non-polar state. Thus, the non-autonomous analysis in this case is equivalent to that of the SubPB model for organization in region IV (Supplementary Fig. 2D-F). Due to the organization in the region where the HSS and the IHSS coexist on the other hand, the Wave-pinning model can explain both, the non-polar and the polar state. Thus, in absence of a signal the quasi-potential landscape is characterized by three minima - one corresponding to the HSS (circle), where the trajectory is trapped, and the other two corresponding to the two IHSS branches (Fig. 2F, G; Supplementary Fig. 3B right). Upon signal addition, the minimum corresponding to the HSS disappears, leaving a one-well quasi-potential landscape of the stable polar state. Signal removal reverts the system to the three-well quasi-potential landscape, however the system remains in the IHSS well. The dynamics of the system is fully characterized by an asymptotic behavior realized through non-autonomous switching between the available steady states. Thus, these polarity models are characterized by a qualitatively different dynamical transitions in comparison to the SubPB model: asymptotic behavior towards the available steady states in contrast to the non-asymptotic, transient dynamics complemented with transient trapping by the dynamical "ghost", which temporarily maintains the system away from the steady state.

Responsiveness to spatial-temporal signals is uniquely enabled by transient dynamics and metastable signaling state in the SubPB mechanism

To investigate the difference in basic polarization features emerging from the different dynamical transitions, we quantified next polarization ratio (pd = $\frac{u_{left}}{u_{right}}$) to steep and shallow gradients (quantified via a percentage difference, $(s_{left} - s_{right}) \times 100$), time to reach stable polarization at a threshold signal amplitude inducing polarization, and polarization ratio to signals with increasing offset. Scaling of the models that reflects physiological time-scales was implemented as in (Jilkine and Edelstein-Keshet, 2011). The RD simulations were performed on a one-dimensional circular domain using periodic boundary conditions.

The simulations showed that for the LEGI- and Turing- models, polarization can be induced even when the gradient steepness is <0.5 $\%\ pd$ between the front and the back of the cell (Fig. 3A). However, the polarization ratio achieved by the LEGI-type model is relatively small (<1), indicating that the LEGI mechanism cannot account for signaling

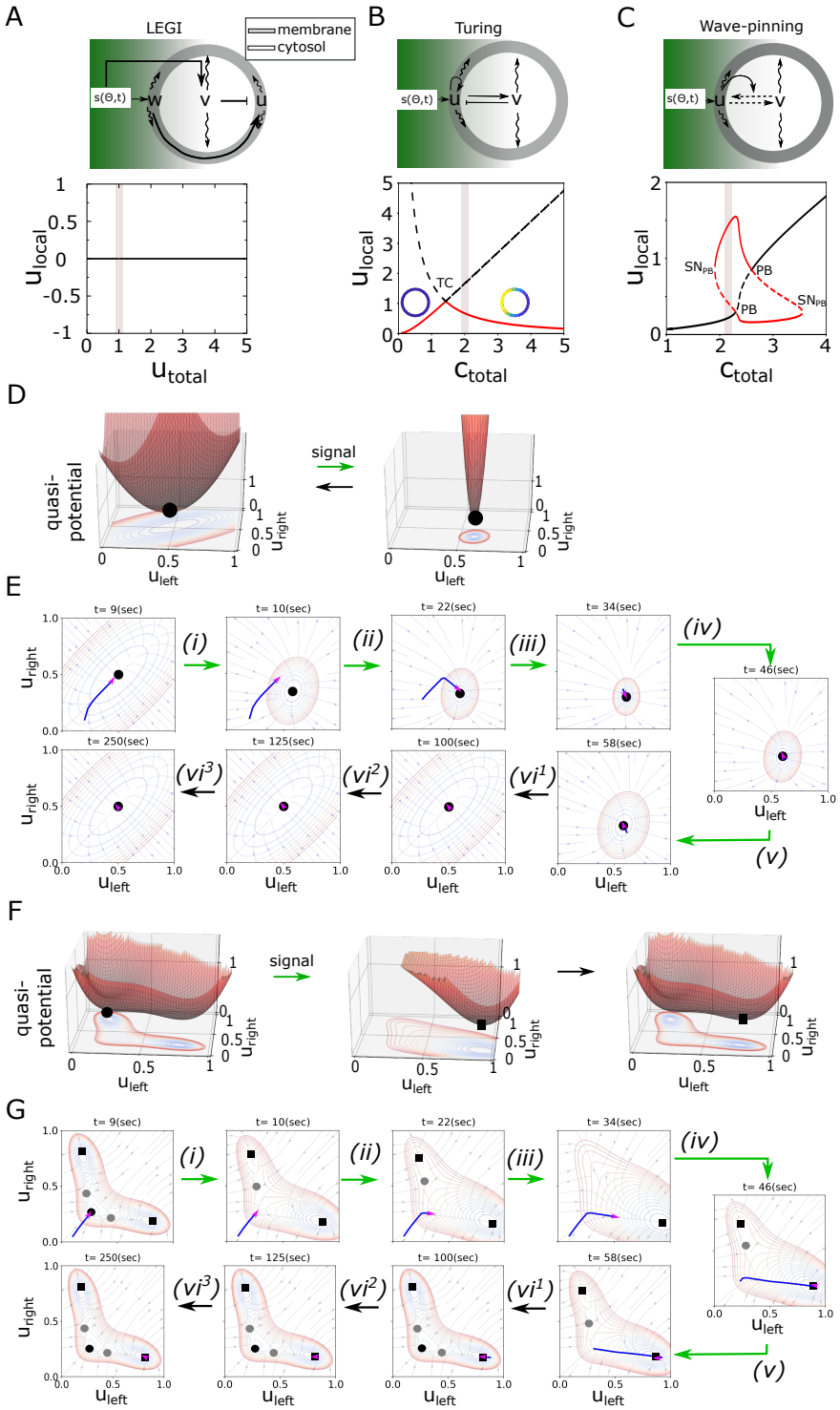

Figure 2: Dynamical characteristics of the LEGI, Turing-like and Wave-pining polarity models. (A) Top: topology of interaction of LEGI model. Color coding and arrows as in Fig. 1A. Bottom: corresponding bifurcation diagram and the respective parameter organization in signal absence ($s(\theta, t) = 0$). (B), (C) same as in (A) but for Turing- and Wave-pinning- models, respectively. Shaded region: parameter organization. TC: Transcritical bifurcation; PB: pitchfork bifurcation; SN_{PB}: saddle-node; u/w are membrane bound, and v - cytosolic component. u_{local}: local variable associated with u from LPA analysis. u_{total}, c_{total}: parameters (details in Materials and Methods). In (A)-(C) bottom, line description as in Fig. 1B. (D) Quasi-potential landscapes calculated for the LEGI model when subjected to a step-like transient gradient signal (as in Fig. 1E). Landscapes in absence and maximal signal strength are shown. Transitions in signal presence/absence: green/black arrows. Coloured contour maps: landscape projection in u_{left}-u_{right} plane. (E) Corresponding instantaneous phase portraits and system's trajectory (as in Fig.1G). Blackcircles: stable steady states. Transitions in signal presence/absence: green/black arrows. (F) and (G) Same as in (D) and (E) only for the Turing-like model. Grey circles: saddles; black squares: IHSS.

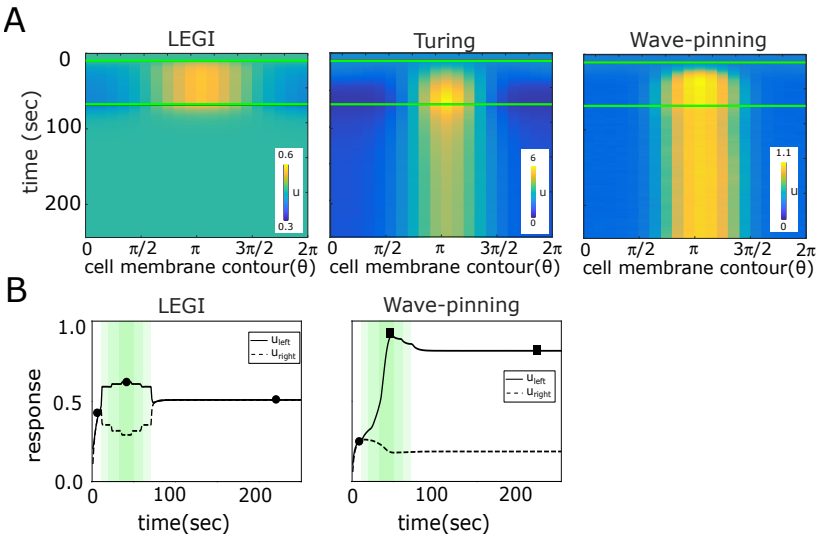

Supplementary Figure 3: Polarization response of the LEGI, Turing-like and Wave-pinning models. (A) Spatial-temporal response (kymographs) of the membrane-bound active component obtained using RD simulations of the LEGI (left), Turing-like (middle) and Wave-pinning (right) models (equations in Materials and Methods). (B) Temporal activity response across the cell's membrane (u_{right}, u_{left}) for the LEGI (left) and the Wave-pinning model (right) upon step-like transient gradient stimulation. Corresponding to Figs.2E,G.

amplification when sensing shallow gradients. This is a direct consequence of the underlying dynamical mechanism: an external signal triggers a continuous and reversible re-positioning of the only stable attractor, and therefore cannot account for signaling amplification. Although the Wave-pinning model effectively generated robust polarization response, it could be triggered even for low gradient amplitudes, indicating susceptibility to spurious activation. This can be explained again by the dynamical structure: due to the organization where HSS and IHSS coexist, a "hard" signal-induced transition effectively results in a threshold activation ($pd_{thresh} = 0.3\%$) and signaling amplification, however the coexistence of both steady states also makes the system susceptible to spurious activation. Spurious activation was also characteristic for the Turing-type model, where it results from organization after the TC, region in which the non-polar state is unstable. Thus, none of these models exhibit reliable threshold activation, and are thereby not robust to noise, suggesting that a unique description of the non-polar state can not be provided. Furthermore, LEGI- and Turing-type models polarized on a time scale longer than 6min, whereas the Wave-pinning model displayed rapid polarization (< 3min, Fig.3B). All models with exception of LEGI can also robustly respond to gradients with off-set (Fig.3C).

In contrast, the equivalent quantification for the SubPB mechanism demonstrated that the critical organization enables sensing steep and relatively shallow gradients, threshold activation and thereby robustness to noisy signal activation (pd_{thresh}=1.2%), rapid polarization times (<3min), and robust polarization to gradients with off-set (Fig. 3A-C, red). SubPB model displays optimal polarization features can be explained with the criticality organization: in absence of a signal, the non-polar state is the only stable steady state, thus threshold activation can be robustly achieved, where as the sub-critical nature of the PB gives rise to the signal amplification to shallow signals. Taken together, these results demonstrate that SubPB enables optimal polarization response.

We next tested the re-polarization capabilities of each of the models by subjecting numerically the cell in the RD simulation to a spatial gradient until stable polarization was achieved, after which the gradient direction was reversed and its steepness increased ($2 \times pd_{thresh}$). The Turing- and Wave-pinning-type models did not re-polarize (in physiologically relevant time-frame, Fig. 3D). This can be understood from the non-autonomous analysis of the system (Fig. 2F,G): the trajectory remained trapped in the symmetry-broken states after signal removal, such that rapid re-polarization cannot be achieved. The LEGI model re-polarized in a time-frame $>$ 3min, but the polarization ratio did not depend on the signal amplitude, as previously shown (Fig. 3B). The SubPB on the other hand, not only enabled rapid re-polarization to spatially reversed gradient signals ($<$ 1 min, Supplementary .Fig 4A), but the polarization response was also sensitive to the amplitude of the reversed signal, as reflected in the polarization amplification. In contrast to the Wave-pinning model, re-polarization for the SubPB mechanism is possible due to organization at criticality - after signal removal, the system is maintained in the dynamical "ghost" state (in contrast to the stable IHSS for the Wave-pinning model), thus the system can rapidly respond to the reversed signal and thereby quickly re-polarize. When presented

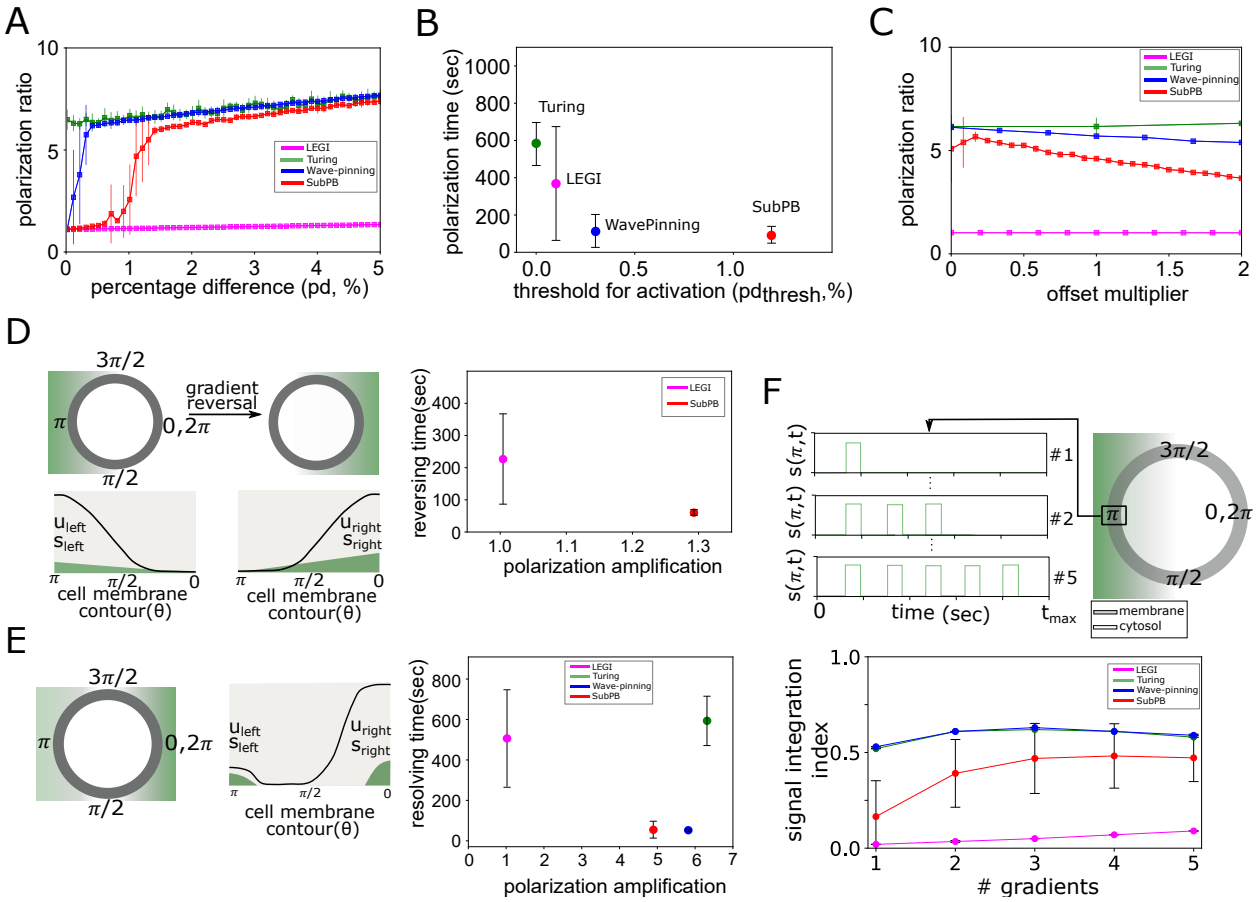

Figure 3: SubPB mechanism enables optimal responsiveness to spatial-temporal chemoattractant signals. (A) Average polarization ratio ($\frac{u_{left}}{u_{right}}$) as a function of percentage difference of the signal across the cell (pd = $(s_{left} - s_{right}) \times 100$)). Mean $\pm$ s.d from 10 RD simulation repetitions. (B) Minimal threshold that activates the system (pd_{thresh}) and time to achieve stable polarization (Materials and Methods). (C) Polarization ratios upon stimulation with a gradient with an offset. (D) Left: schematic representation of gradient reversal across the cell, and respective representation of the spatial profiles of $u(\theta, t)$ and $s(\theta, t)$. Right: Quantification of polarization reversal time and the respective polarization amplification ($\frac{u_{right}}{u_{left}}$) upon stimulation with $\frac{s_{right}}{s_{left}} = 2$. LEGI and Turing-like models did not demonstrate re-polarization in time-interval of 1000 sec. (E) Left: Schematic representation for numerical stimulation protocol with simultaneous signals localized on opposite ends, and corresponding schematic spatial profile of $u(\theta, t)$ and $s(\theta, t)$. Right: Quantification of the time necessary to achieve unique polarization axis and the corresponding polarization amplification, for stimulus ratio $\frac{s_{right}}{s_{left}} = 2$. (F) Top: Schematic representation for numerical stimulation protocol with consecutive gradient stimuli for same direction. Bottom: Corresponding quantification of signal integration index (see Materials and methods). See also Supp. Fig. 4.

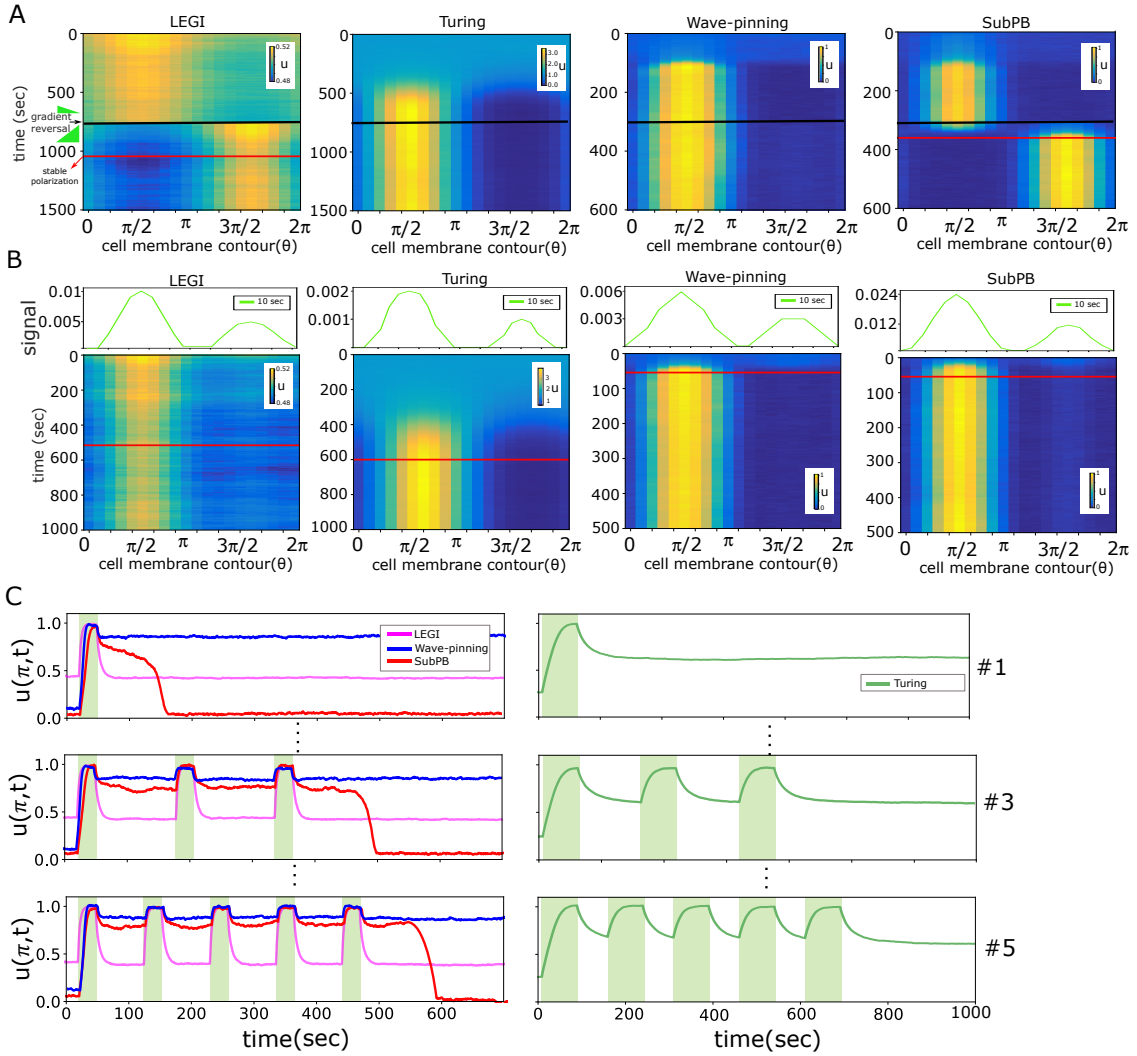

Supplementary Figure 4: Spatial-temporal responses of the four different polarity models. (A) Kymographs depicting the spatial-temporal response of each of the models to reversal of gradient stimuli (black horizontal line). Red horizontal line: time point when stable reversed polarity was established. (B) Kymographs depicting the spatial-temporal response of each of the models stimulated with simultaneous signals with different amplitudes from opposite cell ends. Red horizontal line: time point where stable polarization with unique axis was established. (C) Exemplary temporal response to consecutive signals from same direction (left: LEGI, Wave-pinning and SubPB; right: Turing model). Interval of t=1000 sec. was arbitrarily chosen, temporal profiles remain unaffected over time, as the systems reach the respective steady states.

with two simultaneous, but distinctly localized signals with different amplitudes, only the SubPB and Wave-pinning mechanisms demonstrated effective resolving and rapid and robust polarization in the direction of the stronger signal (Fig. 3E, Supplementary Fig. 4B). This feature in both systems results from the characteristics of the IHSS. In contrast, both LEGI-, Turing- models required more then four times longer time to resolve the signals and polarize in direction of the stronger signal.

We next tested whether the current models can account for temporal memory of recent signal encounters, as demonstrated for SubPB in Fig. 1D. The temporal activity profiles with respect to a spatially localized pulsed stimulus showed that the Wave-pinning- and Turing-type models display prolonged memory of previous signal localization, continuously maintaining the polarized state after the signal removal (Supplementary Fig. 4C, top panel). As described above, this results from maintaining the system's trajectory in polarized state even after signal removal (Fig. 2F,G). Thus, the systems are insensitive to consecutive gradient signal stimulation (Supplementary Fig. 4C, middle an bottom panel) - stimulation with a single or multiple consecutive signals does not change the total duration in which the polarized state is maintained (Fig. 3F). In contrast, the response of the LEGI model rapidly decays after signal removal, demonstrating complete absence of memory, thus the system responds to each gradient independently (Fig. 3F, Supplementary Fig. 4C). The SubPB mechanism on the other hand displays signal-integration features, adapting the polarization duration depending on the number of consecutive stimuli (Fig. 3F, Supplementary Fig. 4C, see Materials and Methods). These results therefore demonstrate that the SubPB mechanism uniquely enables sensing and responsiveness to dynamic signals, as a result of the critical organization that allows utilizing transient dynamics via the presence of a dynamical "ghost" state to adapt to dynamic signals in the environment.

Discussion

We have demonstrated that considering transient dynamics and explicit time-dependence is necessary to describe cellular responsiveness to spatial-temporal chemoattracatnt signals. The current models in the literature rely on an autonomous system's description, where the system's topology determines the number, stability and type of available steady-states, whereas the external signals are thought only to induce switching between them. Mathematically, the description of the asymptotic behavior at or near a steady state is also attractive, as it provides a tractable analysis of the system, since linear stability analysis can be employed to examine the overall dynamical repertoire (Guckenheimer and Holmes, 1983). However, this view only accounts for robustness of regulatory processes, ignoring the temporal system's changes. As we have shown here, the steady-state view cannot account for cellular responsiveness to dynamic cues or how cells resolve simultaneous signals, crucial features of cells that operate in the dynamic environments of tissues and organs.

In contrast, one of the basic characteristics of non-autonomous systems is that the quasi-potential landscape is dynamic itself under time-varying signals, resulting in changes in the number and stability of the steady states. These landscape changes thus guide the movement of the system's trajectory, which can be thereby maintained away from the asymptotic attraction of the available steady states. Effectively, a non-asymptotic transient behavior emerges that enables the system to maintain both robustness in responses (i.e. by transient trapping or slow motion in specific landscape region), while maintaining flexibility in responses to upcoming cues. Recent experimental evidence has demonstrated that indeed, cell's protein activity dynamics is maintained away from steady state, thereby enabling them to retain transient memory of the previous signal's localization, while being responsive to newly perceived signals (Nandan et al., 2022).

However, there is no general theory to analyze or formally describe non-asymptotic transient dynamics, and current analysis has been mostly limited to systems with regular external forcing (Rasmussen, 2007), or numerical investigation of simple two dimensional models (Verd et al., 2013). Here, we provide an additional tool (although also applicable mainly to low-dimensional systems) based on quantification of the Gaussian curvature of the landscape and the corresponding point-wise slope distribution, to separate quantitatively asymptotic from non-asymptotic behavior, and importantly, identify manifolds with a specific topology that enable the system to maintain itself for a prolonged period of time away from the steady state. Long non-asymptotic transients have been characterized in neuronal networks and have been particularly informative, not only about the identity and temporal features of the external signals (Mazor and Laurent, 2005), but also about basic forms of learning such as signal associations (Sharpe et al., 2017). Heteroclinic manifolds in neuronal activity phase-space have been proposed as a mechanism that generate such stable, noise resilient transients (Rabinovich et al., 2008). Transient phenomena with much longer time scales have been also described in the context of regime shifts due to anthropogenic global changes in ecological systems (Hastings et al., 2018). We hereby argue that it is necessary to shift the description of biochemical computations in single cells towards non-autonomous system's description and focus on the role of transient dynamics for processing and interpreting spatial-temporal varying signals.

Acknowledgements

The codes for the numerical simulations will be made available in Github. Funding: The project was funded by the Max Planck Society, partially through the Lise Meitner Excellence Program.

Author contributions

AK conceptualized and supervised the study. AN performed the simulations and analytical work. Both authors interpreted the results and wrote the manuscript.

Competing interests statement

The authors declare no competing interests.

Materials and methods

Analytical description of sub-critical pitchfork bifurcation in spatially extended systems

Let us assume a generalized form of a autonomous RD model of M ($\mathbf{U} \in \mathbf{R}^M$) components in N ($\mathbf{x} \in \mathbf{R}^N$) dimensional space,

$$\frac{\partial \mathbf{U}(\mathbf{x},t)}{\partial t} = \mathbf{F}(\mathbf{U}(\mathbf{x},t)) + \mathbf{D} \cdot \nabla^2 \mathbf{U}(\mathbf{x},t) \tag{3}$$

where $\mathbf{F} \in \mathbf{R}^M$ is the reaction term, $\mathbf{D}$ is a $M \times M$ diagonal matrix of diffusion constants $D_j, j = 1, ..., M$, and ∇^2 is the Laplacian operator. The conditions for a pitchfork bifurcation (PB)-induced transition in a generic RD model therefore must be formally defined.

Let $\mathbf{U_s} = (u_{is})$ for $i = 1, .., M$, be the stable homogeneous symmetric steady state of the RD system. Consider a linear perturbation of the form,

$$\mathbf{U}(\mathbf{x},t) = \mathbf{U_s} + \delta\mathbf{U}(\mathbf{x})e^{(\lambda t)}, \quad \delta\mathbf{U}(\mathbf{x}) \in \mathbf{R}^M \tag{4}$$

where $\delta\mathbf{U}(\mathbf{x})$ is the spatial and $e^{(\lambda t)}$ is the temporal part of the perturbation.

Substituting Eq. (4) in Eq. (3) yields a linearized eigenvalue equation whose solution can be determined by solving the characteristic equation, $F_\lambda = det(\lambda I_{M\times M} - J_{M\times M}) = 0$. J is the Jacobian matrix of the system defined by

$J_{ij} = \frac{\partial \mathbf{F}_i(\mathbf{U}(x,t))}{\partial U_j}, i = 1, ..., M, j = 1, ..., M$ is evaluated at the homogeneous symmetric steady state.

The system exhibits a PB if (Paquin-Lefebvre et al., 2020) , an odd eigenfunction $\delta\mathbf{U}(\mathbf{x})$ such that $\delta\mathbf{U}(-\mathbf{x}) = -\delta\mathbf{U}(\mathbf{x})$, taken in the limit $\lambda \to 0$, fulfills the condition given by:

$$\lim_{\lambda \to 0} F_\lambda = det(J) = 0. \tag{5}$$

When this condition is satisfied, the symmetric, homogeneous steady state of the system undergoes a PB and an inhomogeneous steady state (IHSS). The IHSS is characterized by two stable branches, which in terms of polarization, correspond to left/right-polarized states, where the orientation depends on the direction of the external signal (Fig. 1B).

To identify whether the PB is of sub-critical type, and thereby identify the presence of a SN_{PB}, a weakly nonlinear analysis of Eq. (3) must be performed to obtain a description of the amplitude dynamics of the inhomogeneous state. This can be achieved using an approximate analytical description of the perturbation dynamics based on the Galerkin method (Becherer et al., 2009; Rubinstein et al., 2012; Bozzini et al., 2015). For simplicity, we outline the steps for a one-dimensional system ($N = 1$).

Given a component of the system (i.e. $u(\theta,t) \in \mathbf{U}$), (1) the amplitude of $u(\theta,t)$ can be written as a superposition of periodic functions (harmonics) and, (2) the amplitude of the resulting harmonics, $u_n(t)$ for $n \neq 1$ can be expanded

as power series of the amplitude of the leading harmonics $u_1(t) = \phi(t)$. Substituting the equation for the amplitude of the leading harmonics into Eq. (3) allows to obtain an equation that describes the evolution of $\phi(t)$. If the resulting equation is of Stuart-Landau type:

$$\frac{d\phi}{dt} = c_1\phi + c_2\phi^3 - c_3\phi^5 \tag{6}$$

with $c_1, c_2, c_3 > 0$, which is equivalent to the normal form of a sub-critical pitchfork bifurcation (Strogatz, 2018), then the identified PB is of sub-critical type.

Example: Analytical treatment of the SubPB model

Let us consider the system Eq. (1) with reaction terms as in Eq. (2). This describes the SubPB/Wave-pinning model (Mori et al., 2008). To perform linear stability analysis and identify the existence of a sub-critical PB, a simplified one-dimensional projection is considered,

$$\begin{aligned}
\frac{du_{left}}{dt} &= f_u(u_{left}, v_{left}) - \tilde{D}_u(u_{left} - u_{right}) = G_1 \\
\frac{dv_{left}}{dt} &= f_v(u_{left}, v_{left}) - \tilde{D}_v(v_{left} - v_{right}) = G_2 \\
\frac{du_{right}}{dt} &= f_u(u_{right}, v_{right}) - \tilde{D}_u(u_{right} - u_{left}) = G_3 \\
\frac{dv_{right}}{dt} &= f_v(u_{right}, v_{right}) - \tilde{D}_v(v_{right} - v_{left}) = G_4
\end{aligned} \tag{7}$$

where the subscripts $left$ and $right$ stand for diametrically opposite sides of the one-dimensional domain (Fig. 1A, bottom). $\tilde{D}_u$ and $\tilde{D}_v$ are the diffusion like terms. Let $\mathbf{U_s} = \begin{bmatrix} u_{left,s} \\ v_{left,s} \\ u_{right,s} \\ v_{right,s} \end{bmatrix}$ be the stable symmetric steady state of the system ($u_{left,s} = u_{right,s}$, $v_{left,s} = v_{right,s}$). Stability of this state can be probed using a linear perturbation of the form $\mathbf{U}(t) = \mathbf{U_s} + \delta\mathbf{U}(t)$ where $\delta\mathbf{U} = \begin{bmatrix} \delta u_{left} \\ \delta v_{left} \\ \delta u_{right} \\ \delta v_{right} \end{bmatrix} \exp(\lambda t)$, is a small amplitude perturbation with growth rate λ. Linearization of the system Eq. (7) results in a Jacobian $\mathbf{J}$ of the form:

$$\mathbf{J} = \begin{bmatrix} \frac{\partial G_1}{\partial u_{left}} & \frac{\partial G_1}{\partial v_{left}} & \frac{\partial G_1}{\partial u_{right}} & 0 \\ \frac{\partial G_2}{\partial u_{left}} & \frac{\partial G_2}{\partial v_{left}} & 0 & \frac{\partial G_2}{\partial v_{right}} \\ \frac{\partial G_3}{\partial u_{left}} & 0 & \frac{\partial G_3}{\partial u_{right}} & \frac{\partial G_3}{\partial v_{right}} \\ 0 & \frac{\partial G_4}{\partial v_{left}} & \frac{\partial G_4}{\partial u_{right}} & \frac{\partial G_4}{\partial v_{right}} \end{bmatrix} \tag{8}$$

where G_1, G_2, G_3 and G_4 are the reaction terms of the one-dimensional projection model. The partial derivatives in $\mathbf{J}$ are evaluated at $\mathbf{U_s}$. The existence of a PB is guaranteed when the eigenvalue λ associated with the odd mode of perturbation given by δu_{left}=$-\delta u_{right}$ and δv_{left}=$-\delta v_{right}$, vanishes. Evaluating the determinant of the Jacobian in Eq. (8) for this odd mode of the perturbation gives,

$$\lim_{\lambda \to 0} F_-(\lambda) = \begin{vmatrix} (\frac{\partial G_1}{\partial u_{left}} + \frac{\partial G_3}{\partial u_{right}}) - (\frac{\partial G_1}{\partial u_{right}} + \frac{\partial G_3}{\partial u_{left}}) & (\frac{\partial G_1}{\partial v_{left}} + \frac{\partial G_2}{\partial v_{right}}) \\ (\frac{\partial G_2}{\partial u_{left}} + \frac{\partial G_4}{\partial u_{right}}) & (\frac{\partial G_2}{\partial v_{left}} + \frac{\partial G_4}{\partial v_{right}}) - (\frac{\partial G_2}{\partial v_{right}} + \frac{\partial G_4}{\partial v_{left}}) \end{vmatrix} = 0 \tag{9}$$

where |.| denotes the determinant of the matrix.

To test the sub-critical nature of the PB, an approximate expression of the amplitude of the symmetry-broken state is derived. As we are interested in the description of a structure of finite spatial size (i.e. finite wavelength k of the symmetry-broken state), the final solution of the system Eq. (1) is expanded around the fastest growing mode, k_m into a superposition of spatially periodic waves:

$$\begin{aligned} u(\theta,t) &= \phi(t)e^{ik_m\theta} + \phi^*(t)e^{-ik_m\theta} + u_0(t) + \sum_{n=2}^{3}(u_n(t)e^{nik_m\theta} + u_n^*(t)e^{-nik_m\theta}) \\ v(\theta,t) &= \phi(t)e^{ik_m\theta} + \phi^*(t)e^{-ik_m\theta} + v_0(t) + \sum_{n=2}^{3}(v_n(t)e^{nik_m\theta} + v_n^*(t)e^{-nik_m\theta}) \end{aligned} \tag{10}$$

where $u(v)_n(t)$ is the complex amplitude of the nth harmonics. The expansion is taken to $n = 3^{rd}$ order, rendering an amplitude equation of 5th order. For simplification, the Hill function in $f_u(u,v)$ is approximated by assuming $(K/u) >> 1$ to yield $f_u(u,v) = (k_0 + \gamma u^2)v - \delta u$. By substituting Eq. (10) in Eq. (3) gives,

$$\begin{aligned} \frac{d\phi}{dt}e^{ik_m\theta} + \frac{du_0}{dt} + .. = k_0(\phi e^{ik_m\theta} + v_0..) + \gamma((3|\phi|^2\phi + 2u_0v_0\phi)e^{ik_m\theta} + 2(u_0+v_0)|\phi|^2 + ...) \\ -\delta(\phi e^{ik_m\theta} + u_0 + ..) - D_u(k_m^2\phi e^{ik_m\theta} + v_0 + ..) \end{aligned} \tag{11}$$

collecting coefficients of harmonics up to first order on either side gives an equation that governs the evolution of the amplitude:

$$\begin{aligned} \frac{d\phi}{dt} &= (k_0 - (D_u k_m^2 + \delta))\phi + 3\gamma|\phi|^2\phi + 2\gamma u_0 v_0 \phi \\ \frac{du_0}{dt} &= (2\gamma|\phi|^2 - \delta)u_0 + (k_0 + 2\gamma|\phi|^2)v_0 \end{aligned} \tag{12}$$

The complex coefficients of the $n = 0^{th}$ harmonics is next approximated as power series of $\phi(t)$ (Becherer et al., 2009):

$$\begin{aligned} u_0(t) &\approx u_0^{(2)}|\phi|^2 + ... \\ v_0(t) &\approx v_0^{(2)}|\phi|^2 + ... \end{aligned} \tag{13}$$

Eq. (13) is then substituted into Eq. (12) giving:

$$\begin{aligned} \frac{d\phi}{dt} &= (k_0 - (D_u k_m^2 + \delta))\phi + 3\gamma|\phi|^2\phi + 2\gamma u_0^{(2)} v_0^{(2)}|\phi|^4\phi \\ \frac{du_0}{dt} &= (2\gamma|\phi|^2 - \delta)u_0^{(2)} - (k_0 + 2\gamma|\phi|^2)v_0^{(2)} \end{aligned} \tag{14}$$

Higher order amplitudes were assumed to be in quasi-steady state, thus $\frac{du_0}{dt} = 0$, rendering $v_0^{(2)} = -u_0^{(2)}$. Substituting this into Eq. (14) yields an approximated expression for ϕ:

$$\frac{d\phi}{dt} = c_1\phi + c_2\phi^3 - c_3\phi^5 \tag{15}$$

where $c_1 = (k_0 - (D_u k_m^2 + \delta))$, $c_2 = 3\gamma$ and $c_3 = 2\gamma(u_0^{(2)})^2$. Eq. (15) is of Stuart-Landau type and represents a normal form of a sub-critical pitchfork bifurcation. Taken together, this guarantees the existence of SN_{PB} for system Eq. (1).

Local perturbation analysis (LPA)

Local perturbation analysis is a method to identify dynamical transitions in spatially-extended system (Veronica, 2009; Holmes et al., 2015). Given that $D_v >> D_u$, and considering the limit $D_u \to 0$, $D_v \to \infty$, the stability of the HSS of a PDE system (i.e. Eq. (1) for $s(\theta, t) = 0$) can be probed with respect to a local perturbation in the form of a narrow peak of the slow variable with a negligible total mass. Thus, the height of this peak can be represented as a local variable ($u_{local}(t)$) that does not spatially spread. Due to the fast rate of diffusion of v, it can be represented by a uniform global quantity $v_{global}(t)$. Since u does not spread and v is uniform on the domain, u can then be represented on the remainder of the domain (away from the perturbation) by a global quantity, $u_{global}(t)$, which for mass-conservation systems as in Eq. (1) also captures the evolution of $v_{global}(t)$:

$$\begin{aligned} \frac{\mathrm{d}u_{local}}{\mathrm{d}t} &= f_u(u_{local}, (c_{total} - u_{global})) \\ \frac{\mathrm{d}u_{global}}{\mathrm{d}t} &= f_u(u_{global}, (c_{total} - u_{global})) \end{aligned} \tag{16}$$

Such systems can be further analyzed by means of classical (numerical) bifurcation analysis.

Equations and parameters of different cell polarity models

The Wave-pinning and SubPB models are both described by Eq. (1), with reaction term Eq. (2). For the Wave-pinning model, the parameters were chosen as in (Mori et al., 2008): $k_0 = 0.067s^{-1}, \gamma = 1s^{-1}, K = 1\mu M, \delta = 1s^{-1}$, $c_{total} = 2.25\mu M$. For the SubPB model, c_{total} was chosen to correspond to the critical organization before SN_{PB}, $c_{total} = 2.21\mu M$.

Turing model

For the Turing-like model, the reaction term was taken from (Otsuji et al., 2007) (Model I):

$$f_u(u, v) = a_1(v - \frac{(u+v)}{(a_2(u+v)+1)^2}) \tag{17}$$

Parameters: $a_1 = 2.5$, $a_2 = 0.7$ and $c_{total} = 2$. The external signal $s(\theta, t)$ was introduced same as in Eq. (1), in contrast to (Otsuji et al., 2007), where $s(\theta, t)$ was introduced in the denominator of the reaction term ($(a_2 s(\theta, t)(u + v) + 1)^2$).

LEGI model

The LEGI-type model system is characterized by an incoherent feed forward loop topology, where w is the membrane bound activator, v is the cytosolic inhibitor and u is the membrane bound response component (Levchenko and Iglesias, 2002). The equations are given by,

$$\begin{aligned} \frac{\partial w(\theta, t)}{\partial t} &= f_w(w) + k_w s(\theta, t) + D_w \frac{\partial^2 w}{\partial \theta^2} \\ \frac{\partial v(\theta, t)}{\partial t} &= f_v(v) + k_v s(\theta, t) + D_v \frac{\partial^2 v}{\partial \theta^2} \\ \frac{\partial u(\theta, t)}{\partial t} &= f_u(w, u, v) + D_u \frac{\partial^2 u}{\partial \theta^2} \end{aligned} \tag{18}$$

with

$$f_w(w) = -k_{-w}w$$
$$f_v(v) = -k_{-v}v$$
$$f_u(w,u,v) = k_u w(u_{total} - u) - k_{-u}vu$$

$s(\theta,t)$ is the external stimulus. Parameters: $k_u = k_{-u} = 2s^{-1}$, $k_v = k_{-v} = 1s^{-1}$, $k_w = k_{-w} = 1\mu M^{-1}s^{-1}$, $u_{total} = 0.1\mu M$ (bifurcation parameter) and diffusion coefficients $D_v = 10\mu m^2 s^{-1}$, $D_u = D_w = 0.5\mu m^2 s^{-1}$.

Applying LPA on this system, we obtain:

$$\begin{aligned}
&\frac{\mathrm{d}w_{local}}{\mathrm{d}t} = f_w(w_{local}); \frac{\mathrm{d}w_{global}}{\mathrm{d}t} = f_w(w_{global}) \\
&\frac{\mathrm{d}v_{global}}{\mathrm{d}t} = f_v(v_{global}) \\
&\frac{\mathrm{d}u_{local}}{\mathrm{d}t} = f_u(w_{local}, u_{local}, v_{global}) \\
&\frac{\mathrm{d}u_{global}}{\mathrm{d}t} = f_u(w_{global}, u_{global}, v_{global})
\end{aligned} \tag{19}$$

The **one dimensional projection** of LEGI model is given by,

$$\begin{aligned}
\frac{du_{left}(t)}{dt} &= f_u(w^{qss}_{left}, u_{left}, v^{qss}) - \tilde{D}_u(u_{left} - u_{right}) \\
\frac{du_{right}(t)}{dt} &= f_u(w^{qss}_{right}, u_{right}, v^{qss}) - \tilde{D}_u(u_{right} - u_{left})
\end{aligned} \tag{20}$$

with

$$v^{qss} = 0.5\frac{k_v}{k_{-v}}(s_{left} + s_{right})$$
$$w^{qss}_{right} = \frac{k_w}{k_{-w}}(s_{left} + s_{right}) - w^{qss}_{left}$$
$$w^{qss}_{left} = \frac{k_w}{(2\tilde{D}_w + k_{-w})}(s_{left} + \frac{\tilde{D}_w(s_{left} + s_{right})}{k_{-w}})$$

This two component simplification was obtained from Eq. (18) after a quasi-steady state approximation of v and w.

Bistable model

A two component diffusing toggle switch model is considered:

$$\begin{aligned}
\frac{\partial u(\theta,t)}{\partial t} &= f_u(u,v) + D_u\frac{\partial^2 u}{\partial \theta^2} + s(\theta,t) \\
\frac{\partial v(\theta,t)}{\partial t} &= f_v(u,v) + D_v\frac{\partial^2 v}{\partial \theta^2}
\end{aligned} \tag{21}$$

with

$$f_u(u,v) = (u_T - u)(a_1(u_T - u) + a_2 u) - g_1 uv$$

$$f_v(u,v) = k_1(v_T - v) - k_2 v - b_1 uv$$

and parameters: $a_1 = 0.001, a_2 = 1.9, b_1 = 11, k_1 = 0.5, k_2 = 0.5, v_T = 1, u_T = 1.35$. Maximum amplitude of signal was set to 0.04.

Estimating quasi-potential landscapes

In order to obtain the quasi-potential landscapes for the systems Eq. (7) and Eq. (20), the method described in (Wang et al., 2010) is adopted. For non-equillibrium systems, the underlying potential that defines the state-space flows cannot be obtained by integrating the force terms (the reaction terms of the ODE system). This issue can be bypassed by introducing stochasticity into the system. In a stochastic system, each state **x** (here **x**$= (x, y) = (u_{left}, u_{right})$) is described using a probability in time and state space position **x**, P(**x**, t). The time evolution of the P(**x**,t) not only depends on the forces that drive the system, but also the stochastic transitions between adjacent points in the state space. This can be formalized using a Fokker-Planck equation that captures the interplay between deterministic and stochastic nature of the system and is given by,

$$\frac{\partial P(u_{left}, u_{right}, t)}{\partial t} = -\frac{\partial (G_1 P)}{u_{left}} - \frac{\partial (G_3 P)}{u_{right}} + (\frac{\partial^2}{\partial u_{left}^2} + \frac{\partial^2}{\partial u_{right}^2})(DP) \tag{22}$$

where D is the diffusion constant associated with stochastic transitions, G_1 and G_3 are the reaction terms of u_{left} and u_{right} from one dimensional projection models Eq. (7) and (20). By numerically solving Eq. (22), the asymptotic state of the probability distribution, P_{ss}, given by the limit P(**x**, $t \to \inf$), is estimated. Analogous to the equillibrium state, an approximate expression for the quasi-potential is then given by, $Q(\mathbf{x}) \approx -ln(P_{ss})$. The Fokker-Planck equations were solved numerically using the python package provided by (Holubec et al., 2019), with $D = 0.02$. The two dimensional grid on which the system is solved has a spatial step size 0.02.

The Gaussian curvature K of the landscapes is given by:

$$K(x, y) = \frac{Q_{xx} Q_{yy} - Q_{xy}^2}{(1 + Q_x^2 + Q_y^2)^2} \tag{23}$$

where $Q_x = \frac{\partial Q}{\partial x}, Q_{xx} = \frac{\partial Q_x}{\partial x}, Q_y = \frac{\partial Q}{\partial yy}, Q_y = \frac{\partial Q_y}{\partial y}, Q_{xy} = \frac{\partial Q_x}{\partial y}$ are the first and second order partial derivatives of the quasi-potential surface. State space regions with positive K values were identified using a threshold given by $K_{mean} + 0.1K_{std}$. The boundary that determines the asymptotic behavior of the trajectory in the vicinity of a steady state, Q_{bound}, is estimated as the mean of the quasi-potential values at the boundary of the identified region that satisfies the condition that the slopes are distributed around zero (Fig. 1F).

Model implementation

The models were implemented using a custom-made Python code. One dimensional domain of length $L = 2\pi R$ with $R = 2$ was divided into 20 equal bins and the spatial diffusion terms containing second derivatives were approximated by centered finite difference method. This converted the PDEs into a set of ODEs. Using these ODEs, stochastic simulations were performed using Python SDE solver *sdeint* with noise intesity σ=0.005 for Wave-pinning-, Turing- and SubPB models, and $\sigma = 0.0005$ for the LEGI-type model. Periodic boundary condition is used for all the simulations. For each model, initial conditions are chosen to be around the homogeneous steady steady state. The stimulus gradient was implemented using a Gaussian function of the form $s(\theta) = s_0 e^{\frac{-\theta^2}{2\sigma^2}}$, where s_0 and σ determine the magnitude and spread of the signal.

Model comparison

In order to compare polarization features arising from the different types of dynamical mechanisms, we quantified several metrics: polarization ratio to steep and shallow gradients quantified via a percentage difference (described in the main text), time to reach stable polarization at a threshold signal amplitude inducing polarization, polarization ratio to signals with increasing offset, time necessary for polarization reversal/resolving simultaneous stimuli and subsequent polarization amplification, and response to consecutive stimuli (using signal integration index). In order to estimate the polarization time (Fig. 3A), $u(\theta, t)$ was normalized between max and min values to enable model comparison. Polarization time was then estimated as the first time point at which the normalized response reaches within a small window ($\pm e^{-2}$) around the mean of the last 100 time points during gradient stimulation. The threshold for activation ($pd_{thesh}, \%$) represents the minimal signal amplitude for which stable polarization was achieved, and was estimated from Fig. 3A as the pd where polarization ratio crosses 50% of the maximum polarization ratio. pd_{thresh} was manually set for the LEGI model to 0.5%, and for the Turing-model to 0.1%, as both systems exhibit spurious activation to noise.

For testing sensing of signals with an offset, maximal signal amplitude was set equal to the offset multiplier times the pd_{thresh} for each of the models. Reversing and resolving times were estimated equivalently to the polarization time. For the reversed polarization in Fig.3D, the Turing and the Wave-pinning models are not depicted, as they exhibited reversed polarization with ration < 1. The **signal integration index** in Fig. 3F is estimated as $\frac{([u_{left,a}]-[s_{left}])}{t_{max}}$ where $[u_{left,a}]$ is the total duration in which $u_{left} > 0.5$, $[s_{left}]$ is the total duration of signal gradient stimulation, and t_{max} is the total simulation time.

References

Barton, L. J., LeBlanc, M. G., and Lehmann, R. (2016). Finding their way: themes in germ cell migration. *Current opinion in cell biology*, 42:128–137.

Becherer, P., Morozov, A. N., and van Saarloos, W. (2009). Probing a subcritical instability with an amplitude expansion: An exploration of how far one can get. *Physica D: Nonlinear Phenomena*, 238(18):1827–1840.

Bozzini, B., Gambino, G., Lacitignola, D., Lupo, S., Sammartino, M., and Sgura, I. (2015). Weakly nonlinear analysis of turing patterns in a morphochemical model for metal growth. *Computers and Mathematics with Applications*, 70(8):1948–1969.

Edelstein-Keshet, L., Holmes, W. R., Zajac, M., and Dutot, M. (2013). From simple to detailed models for cell polarization. *Philosophical Transactions of the Royal Society B: Biological Sciences*, 368:20130003.

Ermentrout, B. (2002). *Simulating, analyzing, and animating dynamical systems - a guide to XPPAUT for researchers and students*. SIAM.

Golubitsky, M. and Schaeffer, D. G. (1985). *Singularities and groups in bifurcation theory*. Springer.

Goryachev, A. B. and Pokhilko, A. V. (2008). Dynamics of cdc42 network embodies a turing-type mechanism of yeast cell polarity. *FEBS Letters*, 582:1437–1443.

Guckenheimer, J. M. and Holmes, P. (1983). *Nonlinear Oscillations, Dynamical Systems, and Bifurcations of Vector Fields*. Springer.

Hastings, A., Abbott, K. C., Cuddington, K., Francis, T. B., Gellner, G., Lai, Y.-C., Morozov, A. Y., Petrovskii, S. V., Scranton, K., and Zeeman, M. L. (2018). Transient phenomena in ecology. *Science*, 361:eaat6412.

Holmes, W. R., Mata, M. A. E., and Edelstein-Keshet, L. (2015). Local perturbation analysis: a computational tool for biophysical reaction-diffusion models. *Biophysical journal*, 108 2:230–6.

Holubec, V., Kroy, K., and Steffenoni, S. (2019). Physically consistent numerical solver for time-dependent fokker-planck equations. *Physical Review E*, 99:032117.

Jilkine, A. and Edelstein-Keshet, L. (2011). A comparison of mathematical models for polarization of single eukaryotic cells in response to guided cues. *PLoS Computational Biology*, 7:1–15.

Lämmermann, T., Afonso, P. V., Angermann, B. R., Wang, J. M., Kastenmüller, W., Parent, C. A., and Germain, R. N. (2013). Neutrophil swarms require ltb4 and integrins at sites of cell death in vivo. *Nature*, 498:371–375.

Levchenko, A. and Iglesias, P. A. (2002). Models of eukaryotic gradient sensing: application to chemotaxis of amoebae and neutrophils. *Biophysical journal*, 82 (1 Pt 1):50–63.

Levine, H., Kessler, D. A., and Rappel, W.-J. (2006). Directional sensing in eukaryotic chemotaxis: a balanced inactivation model. *Proceedings of the National Academy of Sciences of the United States of America*, 103:9766.

Mazor, O. and Laurent, G. (2005). Transient dynamics versus fixed points in odor representations by locust antennal lobe projection neurons. *Neuron*, 48:661–673.

Mori, Y., Jilkine, A., and Edelstein-Keshet, L. (2008). Wave-pinning and cell polarity from a bistable reaction-diffusion system. *Biophysical journal*, 94:3684–3697.

Mori, Y., Jilkine, A., and Edelstein-Keshet, L. (2010). Asymptotic and bifurcation analysis of wave-pinning in a reaction-diffusion model for cell polarization. *SIAM journal on applied mathematics*, 71:1401–1427.

Nandan, A. P., Das, A., Lott, R., and Koseska, A. (2022). Cells use molecular working memory to navigate inchanging chemoattractant fields. *eLife*, 11:e76825.

Otsuji, M., Ishihara, S., Co, C., Kaibuchi, K., Mochizuki, A., and Kuroda, S. (2007). A mass conserved reaction–diffusion system captures properties of cell polarity. *PLoS Computational Biology*, 3:1–15.

Paquin-Lefebvre, F., Xu, B., DiPietro, K. L., Lindsay, A. E., and Jilkine, A. (2020). Pattern formation in a coupled membrane-bulk reaction-diffusion model for intracellular polarization and oscillations. *Journal of Theoretical Biology*, 497:110242.

Parent, C. A. and Devreotes, P. N. (1999). A cell's sense of direction. *Science*, 284:765–770.

Rabinovich, M. G., Huerta, R., and Laurent, G. (2008). Transient dynamics for neural processing. *Science*, 321:48 – 50.

Rasmussen, M. (2007). *Attractivity and bifurcation for nonautonomous dynamical systems*. Springer.

Rubinstein, B., Slaughter, B. D., and Li, R. (2012). Weakly nonlinear analysis of symmetry breaking in cell polarity models. *Physical Biology*, 9(4):045006.

Samara, N. L., Datta, A. B., Berndsen, C. E., Zhang, X., Yao, T., and Cohen, R. E. (2011). The onset of collective behavior in social amoebae. *Science*, 328:1021 – 1025.

Sharpe, M. J., Chang, C. Y., Liu, M. A., Batchelor, H. M., Mueller, L. E., Jones, J. L., Niv, Y., and Schoenbaum, G. (2017). Dopamine transients are sufficient and necessary for acquisition of model-based associations. *Nature neuroscience*, 20:735 – 742.

Shellard, A. and Mayor, R. (2016). Chemotaxis during neural crest migration. *Seminars in cell & developmental biology*, 55:111–8.

Skoge, M. L., Yue, H., Erickstad, M. J., Bae, A. J., Levine, H., Groisman, A., Loomis, W. F., and Rappel, W.-J. (2014). Cellular memory in eukaryotic chemotaxis. *Proceedings of the National Academy of Sciences*, 111:14448 – 14453.

Strogatz, S. H. (2018). *Nonlinear dynamics and chaos: with applications to physics, biology, chemistry, and engineering*. CRC Press.

Verd, B., Crombach, A., and Jaeger, J. (2013). Classification of transient behaviours in a time-dependent toggle switch model. *BMC Systems Biology*, 8:43 – 43.

Veronica, G. (2009). *Dynamics of auxin patterning in plant morphogenesis*. PhD dissertation, University of Utrecht, The Netherlands.

Wang, J., Xu, L., Wang, E., and Huang, S. (2010). The potential landscape of genetic circuits imposes the arrow of time in stem cell differentiation. *Biophysical journal*, 99:29–39.

Welf, E. S., Ahmed, S., Johnson, H. E., Melvin, A. T., and Haugh, J. M. (2012). Migrating fibroblasts reorient directionality by a metastable, pi3k-dependent mechanism. *The Journal of Cell Biology*, 197:105 – 114.

Xiong, Y., Huang, C.-H., Iglesias, P. A., and Devreotes, P. N. (2010). Cells navigate with a local-excitation, global-inhibition-biased excitable network. *Proceedings of the National Academy of Sciences*, 107:17079 – 17086.